(Received 16 December 2025, Accepted 12 January 2026, Scheduled 24 January 2026)

CSRR-Loaded Reconfigurable SIW Bandpass Filter Using p-i-n Diodes for S-Band and 5G n79/C-Band Applications

Amjad A. Al-Rahmah* and Bashar J. Hamza

Department of Communications Technical Engineering, Al-Najaf Technical Engineering College/Najaf Al-Furat Al-Awsat Technical University ATU, Najaf 54001, Republic of Iraq

ABSTRACT: Modern wireless systems require filters capable of independently tuning multiple frequency bands; however, conventional designs lack sufficient flexibility and often exhibit high losses. The proposed filter addresses this limitation by offering a compact, low-loss, and independently reconfigurable dual-band operation suitable for multistandard applications. Accordingly, a reconfigurable substrate-integrated waveguide bandpass filter is presented in this study, which is applicable to wireless systems. The first operating band is centered at 2.7 GHz with a tuning range of 13.4%, whereas the second band is centered at 4.7 GHz and achieves a tuning range of 26.35%. The lower band is intended for S-band applications, whereas the upper band supports 5G band n79 and can be reconfigured to operate within the C-band. The proposed structure employs complementary split-ring resonator slots on the top layer, integrated with four p-i-n diodes. The filter exhibits compact dimensions of $0.21\lambda_g \times 0.48\lambda_g$, an insertion loss below 1 dB, and a return loss of 14 dB. Advanced design techniques, including eigenmode analysis, were utilized to ensure accurate selectivity and coupling matrix extraction. Furthermore, the filter demonstrates strong suppression up to 9 GHz, ensuring low interference. A prototype was fabricated and measured, showing good agreement with simulation results.

1. INTRODUCTION

Radio frequency (RF) filters have frequency-selective transmission characteristics, enabling the passage of acceptable frequencies (passbands) while attenuating unwanted frequencies (stopbands). Microwave filters, in particular, are important components of the front end of contemporary communication systems. The ongoing advancement in wireless communication technologies necessitates RF front-end designs with enhanced performance, reduced power consumption, and a more compact form factor. Traditional nonplanar topologies, such as rectangular waveguides, achieve superior filter performance relative to planar configurations because of their reduced loss characteristics. Nonetheless, planar designs such as microstrip and coplanar waveguide filters have benefits associated with their small dimensions and low production expenses [1, 2].

Yuan et al. [3] describe a dual-band filter whose first passband is tunable, and the second passband is fixed. The tunable band is realized using stepped-impedance resonators (SIRs) loaded with varactor diodes; its center frequency can be varied from 1.23 to 1.53 GHz with an insertion loss between 0.5 and 4 dB. To implement this design, three metal layers are used: varactor diodes are placed at the ends of the SIRs on the top layer to tune the first passband, whereas two slotlines in the middle layer couple signals to and from the resonators, and this layer serves as a common ground. An eighth-mode substrate-integrated waveguide (EMSIW) cavity on the bottom layer generates a fixed second passband. This multilayer arrangement allows for the independent control of the passbands while maintaining a compact structure.

The design by Pal et al. [4] uses a stub-loaded ring resonator with two varactor diodes to achieve independently tunable odd- and even-mode resonances. One varactor diode is placed in the ring to control the odd-mode resonant frequency, whereas the second connects the stub to the ring to tune the even-mode frequency. A transmission line model was used for the theoretical analysis, and a prototype was fabricated using microstrip technology. The first passband can be tuned from 0.69 to 0.88 GHz with a maximum insertion loss of approximately 1.83 dB, and the second passband can be tuned from 2.67 to 3.78 GHz with an insertion loss below 2.02 dB. Because only two varactor diodes are required, the structure remains compact and in low cost, while allowing the independent adjustment of both bands.

The design by Fan et al. [5] implements a compact, reconfigurable bandpass-to-bandstop filter whose operating mode and frequency can be adjusted electronically. The filter uses a p-i-n diode to toggle between the bandpass and bandstop modes. In the bandstop operation, a two-pole notch response is realized by introducing inductive coupling between the two resonators of the notch filter. In the bandpass mode, two pairs of varactor diodes are employed to independently tune the centre frequency f_0 and adjust the external quality factor; the tuning range is approximately 0.79–1.59 GHz for f_0, while the bandstop mode can be tuned from 0.7 to 1.47 GHz. The design also generates a pair of transmission zeros via two distinct signal paths, thereby improving the selectivity. The reported prototype, which occupies a miniaturized area of approximately $0.16\lambda_g \times 0.11\lambda_g$, demonstrates a wide frequency tuning range with good agreement between the simulated and measured results.

* Corresponding author: Amjad A. Al-Rahmah (amjadabdulsatar@atu.edu.iq).

TABLE 1. Characteristics of the proposed dual-band bandpass filter.

Parameter	Value	Parameter	Value
f_{01}	2.390 GHz	RL_1	-23 dB
f_{02}	5.105 GHz	RL_2	-24 dB
Δ_1	3.77%	N_1	1
Δ_2	2.55%	N_2	1

Brown and Saavedra [6] used eutectic gallium-indium (EGaIn) to enable frequency tuning in an SIW quasi-elliptic bandpass filter with a reconfigurable TE_{101} mode 21 cavity resonator. It had four cavities with vias on the corners, which were selectively filled with EGaIn to tune the frequency. The CF could be varied from 7.96 to 8.39 GHz. Brown and Saavedra [7] used fluidic pockets of different dimensions and shapes to tune the CF of SIW cavities. The f_0 was shifted by more than 170 MHz. The operation frequency was 2.4 GHz, and the IL was less than -5 dB. This hybrid filter design provides an advanced solution for achieving high selectivity and miniaturization in dual-band filters. Although minor deviations in frequency response and optimization complexity pose some challenges, they may introduce slight frequency shifts and increase design optimization effort.

This paper presents a compact and highly reconfigurable dual-band bandpass filter (DB-BPF) designed to meet the requirements of modern wireless communication systems, including frequency agility, multiband operation, compact size, low insertion loss, and adaptability to dynamically changing spectrum conditions. The proposed structure employs an SIW cavity to achieve high performance, as described below. It uses a modified complementary split-ring resonator (CSRR) slot as the main resonating element, which is optimized to enhance the coupling and operation frequency control. Multiple p-i-n diodes are integrated into the resonator and coupling paths, enabling a wide reconfiguration over each operating band. A design methodology based on the IL technique, coupling matrices, and eigenmode analysis was applied to model and optimize the filter behavior. The theoretical predictions were verified through full-wave simulations and experimental measurements.

2. DUAL BAND BANDPASS FILTER CONSTRUCTED ON LOADED SUBSTRATE INTEGRATED WAVEGUIDE WITH COMPLEMENTARY SPLIT RING RESONATORS (CSRR)

This section describes the stages of developing a first-order digital bandpass filter. The proposed filter was designed by applying an IL methodology to determine its theoretical response and fundamental lowpass parameters [8]. This approach is commonly used to create single-band Chebyshev bandpass filters of any order, return loss (RL) level, fractional bandwidth (FBW), and CF. However, to adapt this method for designing a DB-BPF, a multimode resonator with independent mode control is required to enable the application of the superposition theorem. The specifications of the proposed bands are listed in Table 1. The parameters for the low-pass prototype were established according to these specifications, and the group delay τ for these bands was computed, as presented in Table 2.

TABLE 2. Calculated parameters of the proposed DB-BPF.

Parameter	Value	Parameter	Value
g_0	1	M_{s1}	0.12166
g_1	2.25210	M_{1L}	0.12166
g_2	1	τ	0.703

In Table 1, f_{01} and f_{02} represent the CFs; Δ_1 and Δ_2 are the FBWs; RL_1 and RL_2 are the RL levels; and N_1 and N_2 are the orders of the first and second bands, respectively. The components of the coupling matrix $[M]$ are dependent on FBW. The coupling matrix ($[M]$) components depend on the FBW.

Subsequently, the coupling element between resonators i and j, denoted as M_{ij}, is obtained by applying.

$$M_{ij} = \frac{f_0}{\mathrm{BW}} \frac{f_m^2 - f_e^2}{f_m^2 + f_e^2} \tag{1}$$

where BW is the operational bandwidth; f_0 is the CF; f_e and f_m are the electrical and magnetic resonance frequencies of the two connected resonators, respectively, which can be determined via eigenmode analysis. According to [8], the rigorous group delay approach is typically employed in filter design to determine the necessary coupling between the input feed line and the first resonator (as well as between the output feed line and the last resonator) in order to obtain the necessary FBW with optimal impedance matching. The following equation was used to compute τ:

$$\tau(w_o) = \frac{4}{\omega_2 - \omega_1} \frac{1}{R} \tag{2}$$

Here, R is the normalized input and output impedances; ω_1 and ω_2 are the limits of the BW; g_i is the ith low-pass prototype parameter; S refers to the source; and L refers to the load. The following subsections discuss the practical implementation of these parameters in this study.

2.1. The SIW Resonator Proposed

The SIW resonator was constructed on a Rogers RO4350 substrate with a dielectric constant ε_r of 3.66, thickness h of 0.508 mm, and loss tangent $\tan\delta$ of 0.004. The resonator has a physical length L and width W, forming a square-shaped cavity, as shown in Figure 1. The cavity walls were realized using metallic vias of diameter $d = 0.4$ mm, arranged with a pitch distance $p = 1.4$ mm, calculated from Eq. (3). The effective width W_{eff} and effective length L_{eff} of the SIW cavity were obtained using the following equations [9]:

$$p \leq 2d \tag{3}$$

$$f_c = \frac{c}{2W\sqrt{\mu_r \varepsilon_r}} \tag{4}$$

$$W_{eff} = W - \frac{d^2}{0.95 \times p} \tag{5}$$

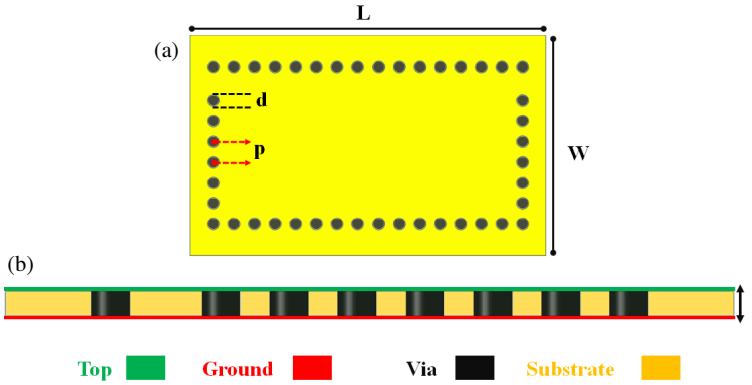

FIGURE 1. Proposed SIW resonator: (a) top and (b) side views.

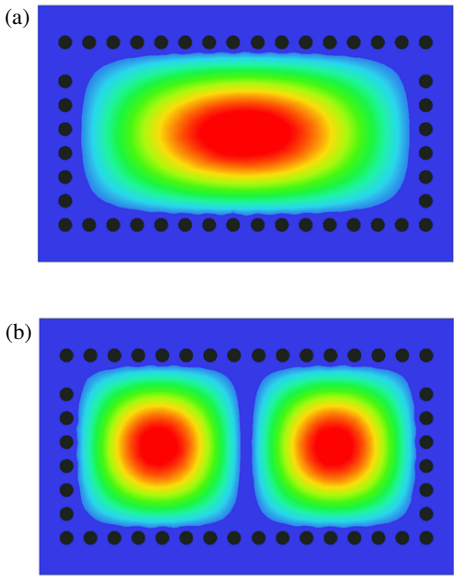

FIGURE 2. Electric field distributions of (a) TE_{10} and (b) TE_{20} modes.

$$L_{eff} = L - \frac{d^2}{0.95 \times p} \tag{6}$$

The eigenmode simulation tool in Ansys EDT was employed to analyze the first two natural modes of the SIW cavities, which would inform the design of the passbands. Using the standard SIW design equations reported in [9] and for dimensions $L = 22.2\,\text{mm}$ and $W = 13.3\,\text{mm}$, the SIW resonator exhibits TE_{10} and TE_{20} modes at frequencies of 8.6 GHz and 10.8 GHz, respectively, with an unloaded quality factor Qu of 250 for each band. The distributions of the electric field (E-field) for these modes are shown in Figures 2(a) and (b), respectively. The appropriate selection of the slot form and dimensions can markedly decrease the resonance frequency and enable independent modulation of various modes.

2.2. Proposed Loaded SIW Resonator with CSRR

The upper layer of the SIW can be loaded efficiently using a slot-like resonator. This slot functions as a control element, allowing such effects to be used for specific shapes and locations. One of the most suitable choices is the use of a CSRR. In this study, a modified CSRR was incorporated to generate two bands. It supports a pair of coupled electric LC modes and has a large effective electrical length owing to the meandering effect; hence, multiple reconfigurable bands are achieved within the proposed structure. The SIW cavity was loaded with CSRR as discussed in [10]. A CSRR was used for several reasons. Because an SIW cavity has multiple modes, each with a different field distribution, the use of a meander slot allows more degrees of freedom to strongly perturb the largest number of these modes independently. Figure 3(a) illustrates the incorporation of the CSRR within the SIW resonator, and Figure 3(b) shows the design parameters of the proposed cavity. To evaluate the effect of the CSRR, multiple eigenmode analyses were conducted by altering the geometric parameters of the proposed slot.

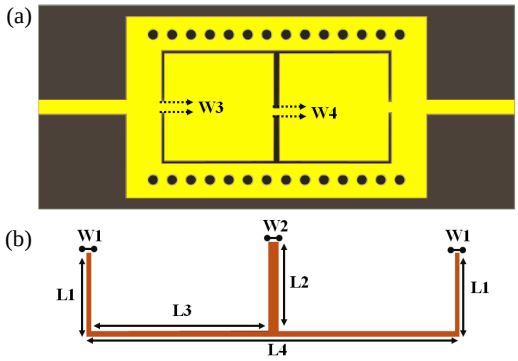

FIGURE 3. Proposed SIW loaded with CSRR: (a) top view, and (b) parameters.

The impact of the distance between the ends of the slot ($W3$) on the first resonance mode 1 ($fr1$) and second resonance mode 2 ($fr2$) is shown in Figure 4. As $W3$ was varied from 0.5 to 7 mm, $fr1$ and $fr2$ increased. However, $W4$ (the distance of the gap in the slot at the center of the resonator) showed a different pattern, because increasing $W4$ led to a large increase in $fr2$, whereas $fr1$ increased only marginally. Varying $W4$ from 0.5 to 7 mm causes $fr2$ to shift toward a higher frequency, as depicted in Figure 5.

The optimal dimensions of the proposed CSRR are $L1 = 3.75\,\text{mm}$, $W1 = 0.2\,\text{mm}$, $L2 = 4.03\,\text{mm}$, $W2 = 0.43\,\text{mm}$, $L3 = 8.09\,\text{mm}$, and $L4 = 17\,\text{mm}$. The CSRR was positioned

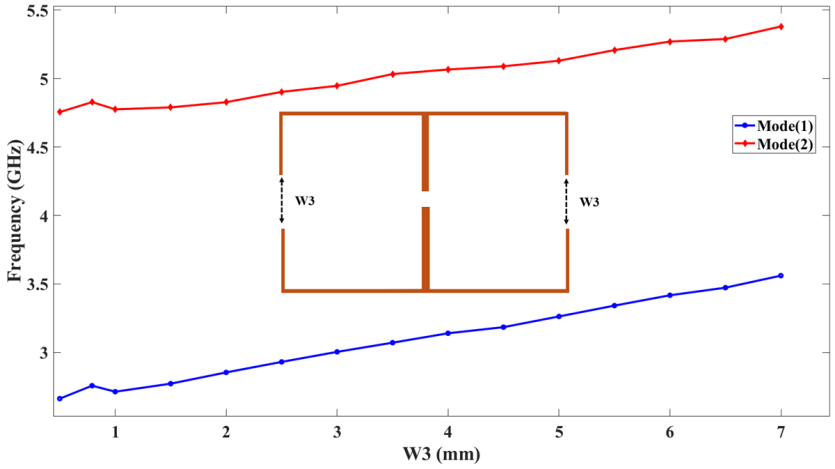

FIGURE 4. Variation in resonance frequencies with $W3$.

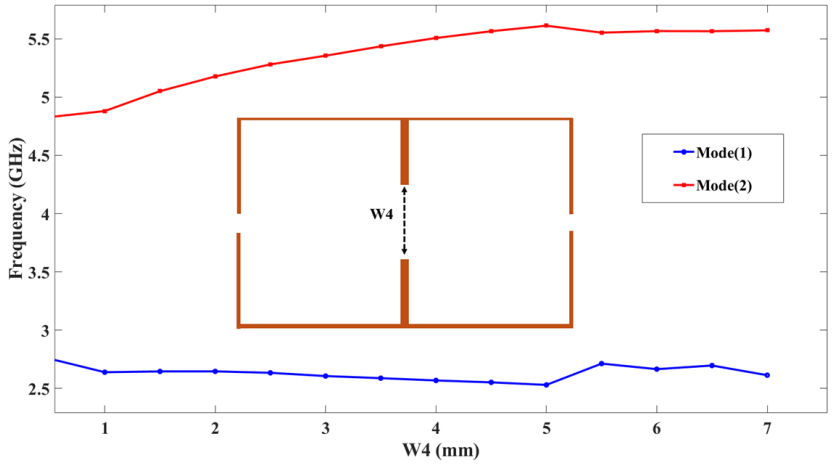

FIGURE 5. Variation in resonance frequencies with $W4$.

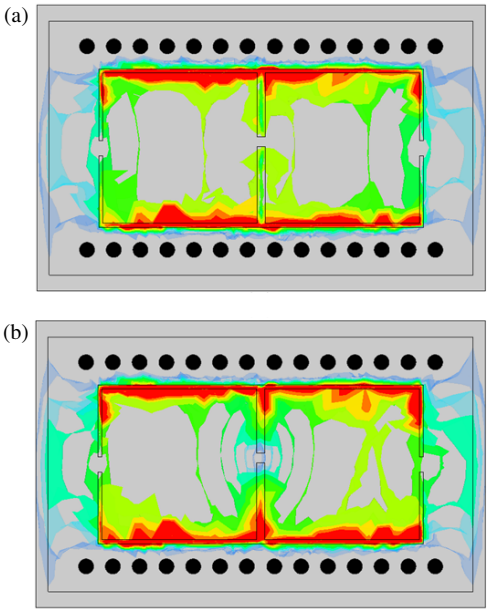

FIGURE 6. EM field distribution of the (a) first and (b) second resonance modes.

away from the edge line on the SIW at a distance of 8.5 mm from the edge. Eigenmode simulation was performed on the finished SIW-CSRR resonator to make the resonance frequencies match the quality factors. The initial mode resonates at 2.67 GHz with $Qu = 268$, and the upper mode resonates at 4.7 GHz with $Qu = 271$, as depicted in Figure 6, it illustrates the field distributions of the resonant modes.

2.3. Reconfigurable Dual-Band SIW Filter

The use of SIW in our design is shown in Figure 7. The overall design contains two coplanar-waveguide feed ports, a CSRR slot, a middle layer made of Rogers RO4350 substrate that is 0.508 mm thick and includes multiple 0.4 mm-diameter vias spaced 1.4 mm from center to center, and a bottom metallic layer that serves as the ground. The design was simulated using a High-Frequency Structure Simulator (HFSS), a commercial finite-element electromagnetic solver. A prototype was fabricated and tested, and the measured results showed good agreement with the simulated response, with slight differences in some cases. The filter exhibits two passbands centered at 2.7 and 4.7 GHz with ILs of approximately 1.5 and 1 dB, respectively. The RLs exceeded 14 dB for both bands. The isolation

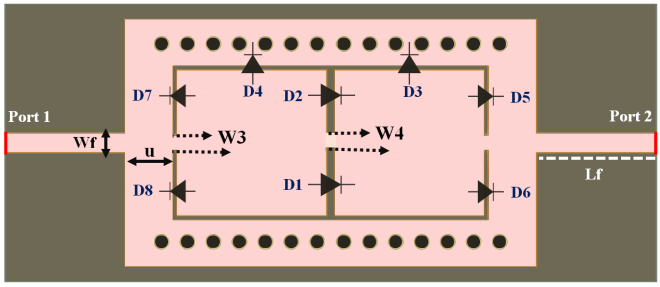

FIGURE 7. Input and output feeding mechanisms of the top view of the structure.

between the passbands was greater than 10 dB, and the out-of-band rejection was greater than 20 dB.

To the best of our knowledge, this is the first time a diode has been placed within the same slot to control the current redistribution process and achieve reconversion of filter tuning. This simplifies the process of controlling the current distribution and facilitates the manufacturing process because it does not require any other modifications to the basic design. The initial intent was to use a diode with a forward bias resistance of less than 0.5 Ω, a reverse bias capacitance of 0.02 pF, and a total diode size of less than 0.2 mm. Because these characteristics are unavailable in the electronic circuit manufacturing market, the diode was replaced with a metal piece. When a forward bias was applied, the piece was placed, and when a reverse bias was applied, it was removed. This practical workaround allowed us to experimentally validate the reconfigurable dual-band response of the proposed SIW filter, whereas a fully diode-integrated implementation with a complete bias network is reserved for future work.

Therefore, two models of the same filter were fabricated. To realize the reconfigurable dual-band bandpass filter shown in Figure 7, four p-i-n diodes, numbered 1–4, were arranged at precisely calculated locations to provide the best filter response. These diodes were manipulated to achieve a reconfigurable CF and transmission zero (TZ) bandpass filter.

Case 1: First, we consider the case in which all the diodes are OFF. In this case, the lower band (B1) is centered at 2.7 GHz and the higher band (B2) at 4.7 GHz, as shown in Figure 8. The field distribution shown in Figure 9(a) confirms that the current is concentrated in the red region around the CSRR slot, with a weaker confinement in the surrounding areas.

Case 2: In this case, D1,2,5,7 are active. The CF of B2 shifts to 6.13 GHz, whereas that of B1 remains unchanged. This implies that B2 can be reconfigured independently of B1. Figure 10 shows the S-parameter for this case, and Figure 9(b) shows the current distribution.

Table 3 lists the measured and simulated IL, RL, and CFs of each band, FBW, and BW for both cases. The TZs in the proposed dual-band SIW filter are mainly generated by the slot-based cross-coupling between the input and output ports because the p-i-n diodes are embedded inside the slot; therefore, their ON/OFF states directly modify the effective coupling path responsible for the signal cancellation and thus influence the locations of the TZs. As the diode configuration changes from

TABLE 3. Reconfigurable SIW filter performance summary (B: Band, S: Simulation, M: measurement).

Case		B1 S.	B1 M.	B2 S.	B2 M.
Case 1	f_0 (GHz)	2.67	3.50	4.72	5.42
	FBW (%)	3.37	5.86	4.45	7.47
	BW(MHz)	90	205	210	405
	RL (dB)	13.22	11.3	19.31	50
	IL (dB)	1.53	2.5	1	2.4
Case 2	f_0 (GHz)	3.09	3.04	6.13	6.08
	FBW (%)	3.56	4.96	8.65	6.94
	BW (MHz)	110	151	530	422
	RL (dB)	12.62	13.35	18.47	14.7
	IL (dB)	1.59	2.7	0.89	1.95

Case 1 to Case 2, the lower and upper TZs shift in frequency. In Case 1, the lower TZ is located at approximately 2.66 GHz, and the upper TZ appears near 4.715 GHz. In Case 2, these TZs move to approximately 3.2 GHz and 6.25 GHz for B1 and B2, respectively, as more diodes are activated. This indicates that the positions of the TZs can be tuned in a controllable manner by adjusting the diode switching states. This controllable movement of the transmission zeros enhances the selectivity on both sides of the passbands.

2.4. Equivalent Circuit of the Proposed Design

The proposed lumped-element equivalent circuit model for the bandpass filter is shown in Figure 11. The metallic via on the SIW wall is modelled as inductance Lg. The input microstrip line coupled to the resonators is represented by $L1$ with $L2$ and $C1$ with $C2$. Each CSRR-slot arm (the conducting paths surrounding the aperture) behaves as the resonator inductance $L6$ with $L7$, and $C5$ with $C6$ denotes the capacitance coupled to the ground through the side openings $W3$. The path between the strip and via wall is modelled as $L3$ and $L4$, and the narrow section above the via wall/central stem of the CSRR is modelled as Lc. The coupling between the two facing resonators occurs through capacitance $L10$ (across the central gap) and magnetic coupling $L11$. The response of the equivalent circuit is illustrated in Figure 12.

3. PROPOSED RECONFIGURABLE FILTER ANALYSIS

The optimized elements of the proposed filter were assembled to construct the final version. To examine the independence of each passband, two different parametric experiments were conducted, and the results are depicted in Figures 4 and 5. The initial analysis, shown in Figure 4, was conducted by varying $W3$. $B1$ and $B2$ exhibited corresponding alterations. The second analysis involved adjusting $W4$ while maintaining a constant value for $B1$, with $B2$ changing independently, as shown in Figure 5. To guarantee a reflection-free transmission of electromagnetic waves at both ends of the filter, the width and length of the inset feed were adjusted. To accurately represent the electrical behavior of the proposed filter, its structural components

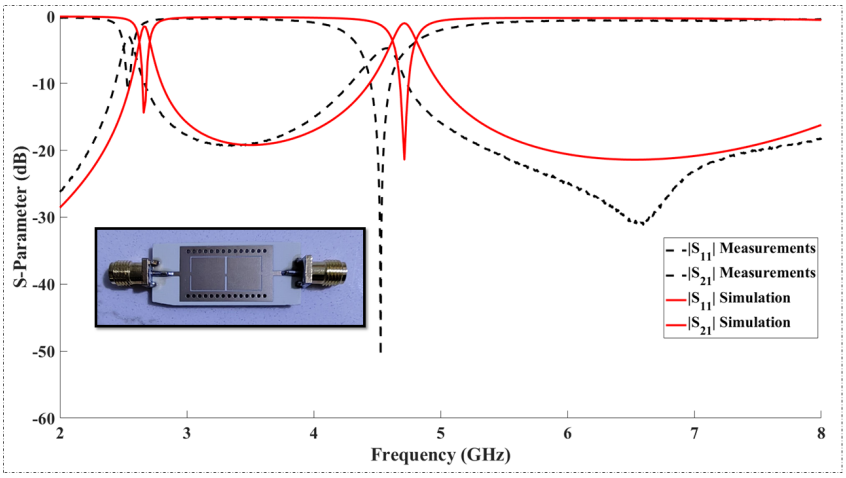

FIGURE 8. Proposed standard design in which all diodes are OFF.

TABLE 4. Final dimensions of the proposed dual-band CSRR slot filter in millimetres.

Parameter	Value	Parameter	Value	Parameter	Value	Parameter	Value
W	13.34	Wf	1.07	$L3$	3.75	d	0.4
$W1$	0.2	$W4$	0.5	$L4$	8.084	P	1.4
$W2$	0.43	$L1$	3.75	Lf	6.5	L	22.2
$W3$	0.79	$L2$	4.23	h	0.508	u	2.72

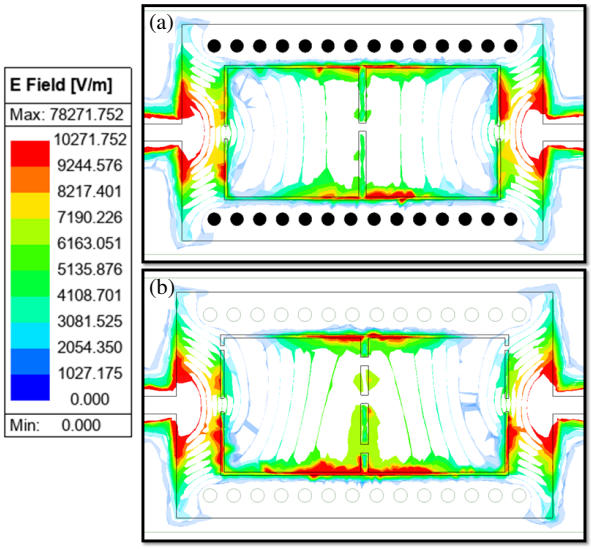

FIGURE 9. Distribution of electromagnetic currents in both cases.

must be defined to develop an equivalent circuit model. Figure 7 shows the proposed SIW CSRR DB-BPF structure with the parameters under study, denoted as W, Wf, and L. The optimized parameters of the proposed filter are listed in Table 4. The overall size of the first-order dual-band SIW CSRR-slot filter was 21 mm $\times$ 34 mm. The realized bands were centred at 2.4 GHz and 5.1 GHz, and the RL was determined to be better than 20 dB over the two cases.

4. SIMULATION AND MEASUREMENT OF THE PROPOSED SIW-CSRR DB-BPF

The fabricated circuit of the proposed SIW CSRR Slot DB-BPF is shown in Figure 13. The fabricated prototype was analysed using the Keysight/Agilent Technologies E5071C vector network analyser (VNA). It was found that the first band has a CF of 2.67 GHz, and the FBW changed from 5.86% to 4.96%, equivalent to a BW from 205 MHz to 151 MHz. The RL is better than 11 dB with an IL of about 2.5 dB. The second band operates at a CF of 5.42 GHz with an FBW varying from 7.47% to 6.94%, equivalent to a BW from 297 MHz to 405 MHz, with the IL less than 2.4 dB and the RL more than 45 dB. The difference in IL level at the two bands is attributed to the impedance matching levels: the first band shows an S_{11} level around 11 dB, whereas the second band shows a lower impedance matching level of $S_{11} = 17$ dB. Furthermore, as the second band operates at a higher frequency band centred at 4.7 GHz, the electrical length of the filter is larger than that at the first band, which is centred at 2.7 GHz, so a higher IL level should be expected at the higher operating band. Accordingly, the two factors contribute to the increase in the IL in the first and second bands. Additionally, the discrepancies between the simulated and measured results were observed. These deviations mainly arise from several practical factors that are not fully captured in the idealized simulations. First, the fabricated prototype employs removable metallic pieces instead of actual p-i-n diodes, which alters the effective slot geometry and introduces contact resistance and parasitic effects, leading to noticeable shifts in the center frequencies. Second, the proposed

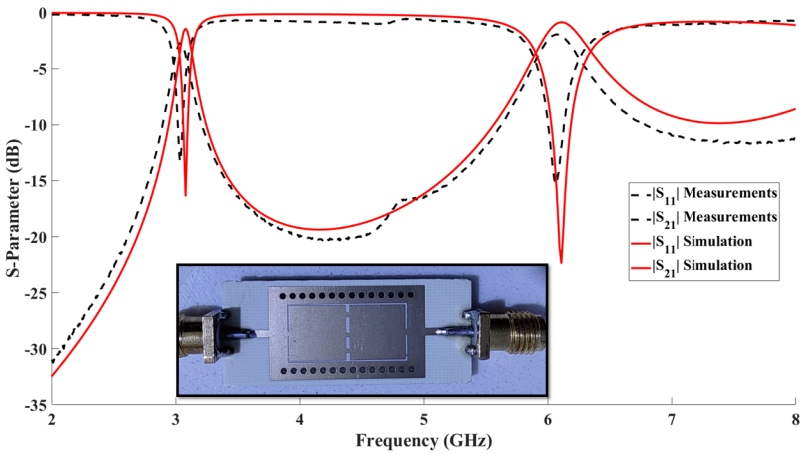

FIGURE 10. Proposed design when diodes 1, 2, 5, and 7 are on.

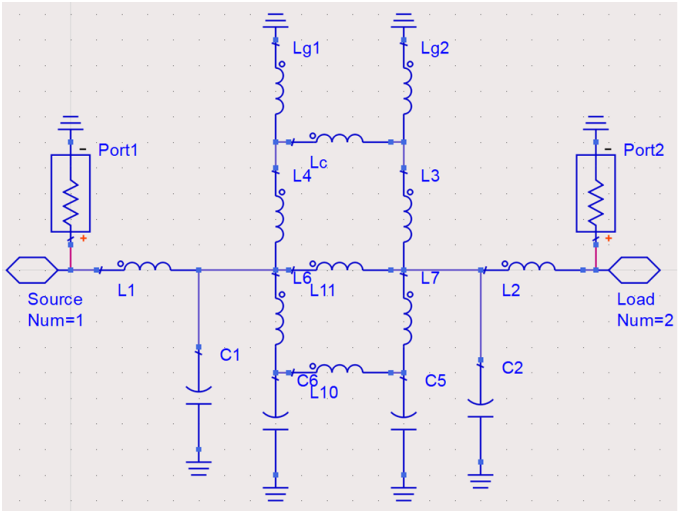

FIGURE 11. Equivalent circuit of proposed filter.

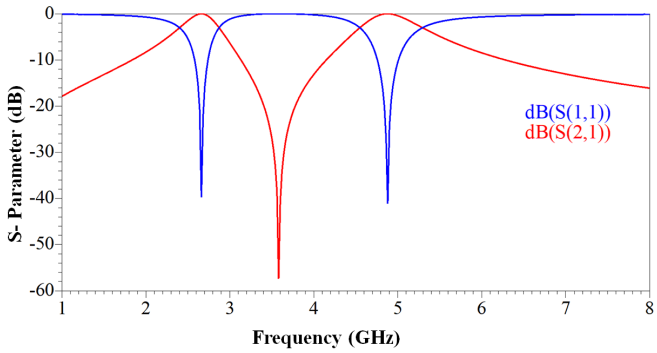

FIGURE 12. LC circuit S-parameter of the DB-BPF.

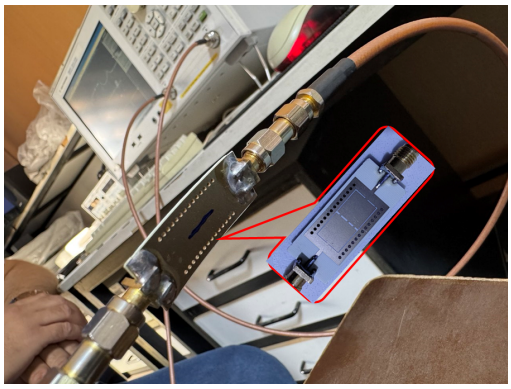

FIGURE 13. Measurements setup.

CSRR-based structure is highly sensitive to small variations in critical slot dimensions, particularly the gap-related parameters, where minor fabrication deviations can result in significant frequency shifts. In addition, the effects of connector launches, feeding transitions, via fabrication tolerances, and conductor surface roughness were not explicitly modeled in the simulations. The combined influence of these factors explains the observed discrepancies and does not undermine the validity of the proposed design methodology.

However, better impedance matching may enhance the IL. Table 5 shows the proposed CSRR slot DB-BPF with the most recent reconfigurable filters.

TABLE 5. Comparison of the proposed CSRR slot DB BPF with other works.

Ref.	F_0 (GHz)	Tuning%	FBW%	S_{11} (dB)	S_{21} (dB)
[11]	3.65/5.8	5.83/11.19	4.72/6.10	> 10	$< 2.9/< 2.1$
[12]	3.1/10.6	51.2	17.69	25	< 1.2
[13]	1.3/1.7	0.8/0.6	12 / 0.8	> 15	< 1.8
[14]	7.86/9.95	9/12.3	9.03/12.35	$> 14/> 12$	< 1.5
[15]	16.2/19.1	1.71/3.09	1.71/3.09	18/19.2	1.8/1.9
[16]	0.209/0.223	4.63/2.74	3.5/3.4	35.3	0.53/1.35
This Work	2.7/4.7	Fix/0.24	(3.37/4.45→6.94)	> 11	$< 2.4/< 2.49$

5. CONCLUSION

The proposed compact dual-band bandpass filter operates at 2.7 GHz for Bluetooth applications and 4.7 GHz for 5G and weather/navigation radar systems. The design provides reconfigurability in both the operating frequency and the TZ, enabling the independent control of the two passbands through tuning mechanisms based on p-i-n diodes. This flexibility enhances its adaptability to multi-standard wireless environments and improves its spectral efficiency. The filter exhibits low ILs and high RLs exceeding 25 dB, making it highly suitable for Bluetooth systems that require low power consumption and efficient signal transmission. Additionally, the structure demonstrates good isolation between the two bands and maintains strong out-of-band rejection up to 9 GHz, ensuring minimal interference with adjacent channels. Fabrication results closely align with simulation outcomes, confirming the robustness and reliability of the proposed reconfigurable architecture. The developed filter is a strong candidate for modern wireless communication systems because of its compactness, tunability, and high-performance characteristics.

REFERENCES

[1] Al-Saedi, H., H. Al-Jeshami, and M. F. Hasan, "Standalone-quad-channels diplexer for modern wireless applications based on overlapped MOERRs," *IEICE Electronics Express*, Vol. 21, No. 19, 20240430, 2024.

[2] Alsultani, A. B., J. G. Chase, and B. Benyó, "Design and validation of substrate integrated waveguide-based blood glucose measurement sensor," *IEEE Sensors Journal*, Vol. 25, No. 11, 20 362–20 373, Jun. 2025.

[3] Yuan, X., W. Kang, H. Zhang, and J. Gao, "Design of tunable balanced dual-band filter using SIR and EMSIW," in *2019 3rd International Conference on Electronic Information Technology and Computer Engineering (EITCE)*, 1646–1650, Xiamen, China, Oct. 2019.

[4] Pal, B., M. K. Mandal, and S. Dwari, "Varactor tuned dual-band bandpass filter with independently tunable band positions," *IEEE Microwave and Wireless Components Letters*, Vol. 29, No. 4, 255–257, Apr. 2019.

[5] Fan, M., K. Song, Y. Zhu, and Y. Fan, "Compact bandpass-to-bandstop reconfigurable filter with wide tuning range," *IEEE Microwave and Wireless Components Letters*, Vol. 29, No. 3, 198–200, Mar. 2019.

[6] Brown, M. and C. E. Saavedra, "Frequency-tunable quasi-elliptic filter using liquid metal," in *2020 IEEE Asia Pacific Conference on Circuits and Systems (APCCAS)*, 110–113, Ha Long, Vietnam, Dec. 2020.

[7] Brown, M. and C. E. Saavedra, "Reconfigurable substrate integrated waveguide circuits using dielectric fluids," in *2020 50th European Microwave Conference (EuMC)*, 542–545, Utrecht, Netherlands, Jan. 2021.

[8] Cameron, R. J., C. M. Kudsia, and R. R. Mansour, *Microwave Filters for Communication Systems: Fundamentals, Design, and Applications*, John Wiley & Sons, 2018.

[9] Al-Darraji, H. and H. Al-Saedi, "Compact dual-band BPF based on loaded SIW with meandered slot line for 5G and beyond applications," *Progress In Electromagnetics Research M*, Vol. 128, 89–98, 2024.

[10] Xiang, Q.-Y., Q.-Y. Feng, X.-G. Huang, and D.-H. Jia, "Substrate integrated waveguide filters and mechanical/electrical reconfigurable half-mode substrate integrated waveguide filters," *Journal of Electromagnetic Waves and Applications*, Vol. 26, No. 13, 1756–1766, 2012.

[11] Iqbal, A., J. J. Tiang, C. K. Lee, N. K. Mallat, and S. W. Wong, "Dual-band half mode substrate integrated waveguide filter with independently tunable bands," *IEEE Transactions on Circuits and Systems II: Express Briefs*, Vol. 67, No. 2, 285–289, Feb. 2020.

[12] Li, Q. and T. Yang, "Compact UWB half-mode SIW bandpass filter with fully reconfigurable single and dual notched bands," *IEEE Transactions on Microwave Theory and Techniques*, Vol. 69, No. 1, 65–74, Jan. 2021.

[13] Simpson, D. J., R. Gómez-García, and D. Psychogiou, "Single-/multi-band bandpass filters and duplexers with fully reconfigurable transfer-function characteristics," *IEEE Transactions on Microwave Theory and Techniques*, Vol. 67, No. 5, 1854–1869, May 2019.

[14] Fang, X., Y. C. Li, L. W. Li, W. Che, and Q. Xue, "A dual-band tunable balanced filter with independently tuning bands," *IEEE Transactions on Circuits and Systems II: Express Briefs*, Vol. 69, No. 4, 2076–2080, Apr. 2022.

[15] Kumar, C. S., R. Kumari, and H. V. Dixit, "Compact dual-band band-pass filter using single multimode SIW cavity with independent controllable fractional bandwidth," *International Journal of RF and Microwave Computer-Aided Engineering*, Vol. 2025, No. 1, 9968988, 2025.

[16] Zhu, B., D. Lu, M. Sun, and M. Yu, "Tunable dielectric filter and filtering power divider with multilevel transfer function tunability," *IEEE Transactions on Microwave Theory and Techniques*, Vol. 73, No. 8, 5133–5151, Aug. 2025.